Available online at www.sciencedirect.com
ScienceDirect
Journal of Nuclear Materials 361 (2007) 62–68
journal of nuclear materials
www.elsevier.com/locate/jnucmat

Evolution of porosity in the high-burnup fuel structure

Antonino Romano [a,*], Matthias I. Horvath [b], Renato Restani [b]

[a] Laboratory for Reactor Physics and Systems Behaviour, Paul Scherrer Institut, CH-5232 Villigen – PSI, Switzerland
[b] Laboratory for Materials Behavior, Paul Scherrer Institut, CH-5232 Villigen – PSI, Switzerland

Received 3 August 2006; accepted 13 September 2006

Abstract

The evolution of the high-burnup structure (HBS) porosity is investigated. Electron probe microanalysis (EPMA) and scanning electron microscope (SEM) measurements of UO_2 fuel with ≈105 GWd/tHM rod average burnup show the formation of an ultra-high burnup structure with a local burnup of 300 GWd/tHM in the proximity of the fuel–cladding interface. Such structure is characterized by gas pores of sizes up to 15 μm. A large population of pores with 3–5 μm pores is also observed in more inner regions of the HBS. An analysis of the pore size distributions indicates predominance of 3.5 μm and 7.5 μm pores. A simple model accounting for vacancy diffusion kinetics and coalescence is used to interpret the observations: the 3.5 μm pores are obtained by growth of 1 μm pores with an initial overpressurization of 50–70 MPa. The extra-large pores with diameters ≈7–8 μm result by coalescence of the intermediate size pores, assuming that: (1) such pores are only slightly overpressurized and that (2) the coalescence process occurs at constant porosity, as observed experimentally.

PACS: 28.41.Ak; 61.18.–j

1. Introduction

The economic advantage of operating fuel at extended burnups has motivated a large scientific effort devoted to the characterization and modeling of the high-burnup fuel structure (HBS), with the purpose of understanding the modifications of the fuel thermal–mechanical performance occurring after restructuring [1–3]. Two key phenomena dominate the fuel behavior at high burnups: (1) the formation of sub-micron grains and (2) the presence of micrometer porosity [1]. While the mechanisms of formation of such microstructures are still open to debate [4,5], theoretical consensus and experimental evidence exist on their evolution under irradiation. In particular, the porosity is observed to increase with burnup and the presence of 'extra-large' pores (with sizes of 4–10 μm or more) in very high burnup samples has been detected [6]. Understanding the evolution of porosity during irradiation is of paramount importance since the porosity directly affects the thermal conductivity and the mechanical strength of the fuel [7,8].

In this paper, experimental and theoretical analyses are presented that investigate the evolution of

* Corresponding author. Present address: ENUSA Industrias Avanzadas, S.A., C. Santiago Rusiñol 12, 28040 Madrid, Spain. Tel.: +34 913 474 456; fax: +34 913 474 421.
E-mail address: antonino.romano@enusa.es (A. Romano).

0022-3115/$ - see front matter © 2006 Elsevier B.V. All rights reserved.
doi:10.1016/j.jnucmat.2006.09.016

micrometer porosity in UO_2. EPMA and SEM observations performed at the Paul Scherrer Institut (PSI) on fuel with very high burnup (≈105 GWd/tHM) yield information on the distribution and morphology of the porosity as well as measurements of local burnups. Specifically, an 'ultra-high burnup' structure is observed to form featuring extra-large pores with sizes of ≈7.5 μm in the very rim region. Moreover, pores of sizes ≈3.5 μm are also observed in more internal regions of the high-burnup structure. To describe the evolution of such porosity in the fuel, a simple model of high burnup porosity is developed, which includes kinetic mechanisms of pore growth due to vacancy diffusion and a simple pore coalescence equation.

This paper is organized as follows: the next section provides information on the experimental technique used to characterize the high-burnup fuel. Then, results are presented starting from a discussion of the main outcomes of the measurements, followed by the analytical model, which is introduced to interpret the observations. Finally, the main findings of this study are summarized in the conclusions.

2. Experimental technique

Experimental observations of high burnup fuel porosity were performed by a shielded electron probe microanalysis (EPMA) of CAMECA CAMEBAX SXR SX-50 with wave length dispersive spectrometers. Furthermore, scanning electron microscope (SEM) images of the high-burnup fuel were taken with this system. Table 1 reports details on the technical specifications of the probing apparatus.

The sample analyzed in this work came from a rod of a commercial Swiss PWR, which had accumulated a peak discharge burnup of ≈105 GWd/tHM and had an initial enrichment of 3.5 wt%. The sample preparation consisted of cutting a thin segment of ≈2 mm thickness, which was embedded with epoxy resin in a steel sample holder and polished to a surface smoothness of 0.25 μm. The measurements were performed on three positions in the rim: two adverse points came from a quantitative line scan over the whole fuel diameter and the third point was perpendicular to the preceding two points. The EPMA measurements yielded information on the elemental distribution of the sample within a depth of 1.0–1.5 μm from the surface. Furthermore, quantitative analyses and SEM pictures were obtained on the same rim locations. Thus, information was obtained on the local concentration of plutonium (Pu) and fission products, such as barium (Ba), cesium (Cs) and neodymium (Nd). To quantify the elemental distributions, the data were calibrated and normalized using the SAMx software [9]. Moreover, care was taken in the measurements in order to avoid disturbances by measuring pores or bubbles in which the elemental concentrations cannot be determined.

3. EPMA and SEM observations

In this section, we present the results of the EPMA and SEM measurements. Fig. 1(a) shows a SEM picture taken from one of three perpendicular positions in the rim of the very high-burnup fuel considered in the analysis. At the fuel–cladding interface, which has a thickness of about 15–25 μm, the fuel is bonded to the cladding and the porosity is relatively low as only a small number of pores with sizes up to ≈5 μm is recorded. The observed finger-like structure of the bonded region could be due to the build-up of contact pressure between fuel and cladding caused by fuel swelling, which is also responsible for gap closure. Inside the fuel, we observed the formation of a region with very large pores starting 5–15 μm from the fuel–cladding interface. These pores have diameters ranging from 5 μm up to 15 μm. Moreover, the local

Table 1
Operating parameters of the shielded CAMECA SX-50 EPMA instrument

High voltage electron beam	20 kV
Beam current	150 nA (±0.5 nA, measured after each point)
Beam diameter	0.5 μm
Lateral resolution for X-rays	2 μm
Scanned area (preselected, stepwise)	11×7 μm^2 typically for each point of direction 1, in the rim zone even less. Point analyses in line scans: 1×1 μm^2 or 1.5×1.5 μm^2
X-ray mappings	50×50 μm^2 with beam scanning (256×256 pixels) Acquisition time: 30 min for each element couple

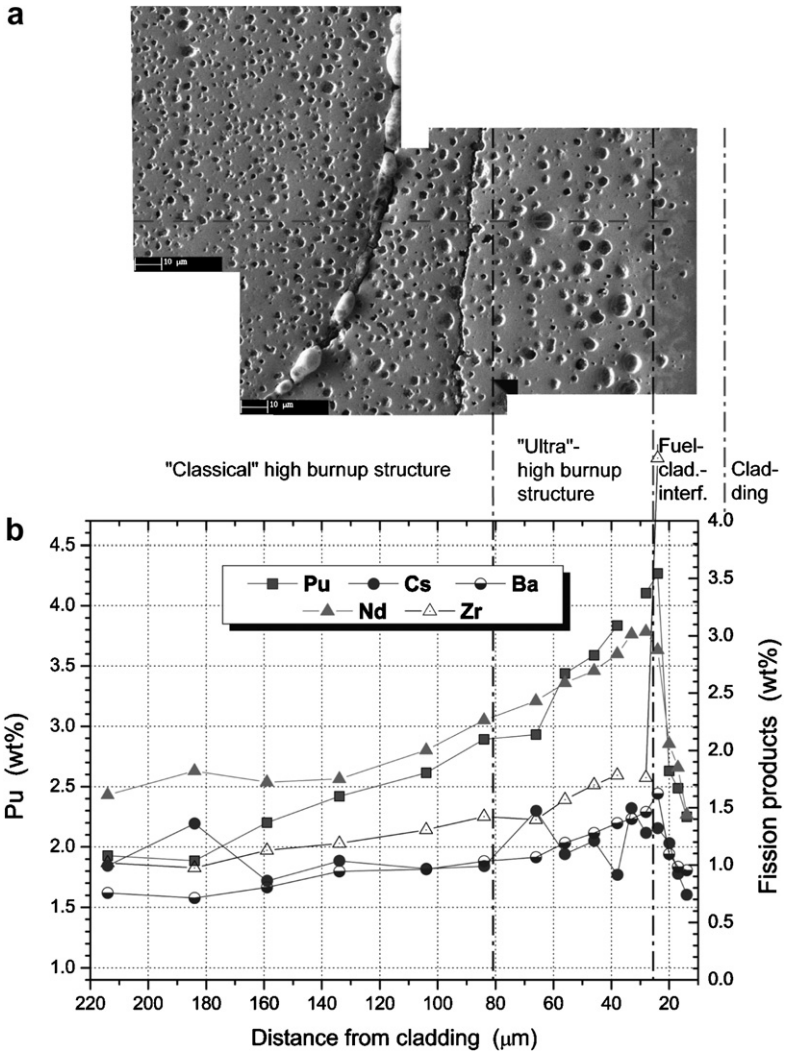

Fig. 1. (a) SEM image of the rim zone and (b) elemental distribution as a function of the distance from the fuel–cladding interface. The elemental analysis was performed along the horizontal dashed line of the SEM snapshot.

porosity is about 22%. Such fuel region, which we call 'ultra-high burnup structure' (UHBS) extends into the fuel for 50–70 μm and is characterized by a strongly reduced pore number density compared to the classical HBS. Moreover, the burnup in this region is up to three times higher than the rod burnup and it decreases rapidly to a level slightly above the pellet average burnup over a few tenths of micrometers. After the UHBS, the standard HBS is observed, which is characterized by a thickness of ≈1 mm and by a local porosity comparable to that of the UHBS. A transition zone is also visible after the HBS up to 2 mm inside the fuel. Finally, in the inner locations, the fuel is not-restructured (these last two regions are not shown in Fig. 1(a)).

The quantitative measurements related to this part of the HBS are reported in Fig. 1(b) and give flat Nd and Pu distributions over much of the fuel radial positions except in the last 200–300 μm towards the fuel rim. In this region, the Nd concentration increases from 1.2 wt% up to 3.1 wt% and the Pu concentration from 1.3 wt% to 4.3 wt%. These values correlate with an estimated local burnup of ≈120 GWd/tHM in the inner flat region and to a burnup of ≈300 GWd/tHM near the fuel–cladding interface. As expected, we observe a sharp drop of these isotopes concentration in the bonded region, where the concentration of zirconium atoms starts to rise. In fact, such region is characterized by a mixture of zirconium oxide, fuel

and fission products. Therefore, the interaction with cladding material leads to a dilution of the plutonium and fission products concentrations.

Fig. 2 shows another SEM picture of the fuel rim region taken at a different position from that reported in Fig. 1(a). Three classes of pore sizes can be identified: standard pores of ≈1 μm (class A) distributed over the entire restructured region, but primarily in the HBS, pores of intermediate size ≈3–5 μm (class B) and extra-large pores (class C) with diameters up to 15 μm located predominantly in the UHBS. The last two pore classes have been more closely analyzed in order to derive histograms yielding the number of pores as a function of their size.

Several pictures taken from different locations in the rim region have been analyzed to count the number of pores of different size classes produced in the HBS, in order to generate distributions of pore sizes. These are shown in Fig. 3. We notice that the intermediate pore size distribution ranges from 2 μm to 6 μm and peaks at about 3.5 μm. The extra large pores are much less numerous and are characterized by a wider size distribution peaked at around 7.5 μm and extending to diameters up to ≈15 μm. Furthermore, the average ratio of class C to class B pores estimated from Fig. 3 is about 15%. An integration of the two histograms gives that the porosity does not change appreciably between the two HBS regions characterized by these pore classes. The observed constant porosity suggests that the class C pores may be formed by coalescence processes. Such conclusion is further discussed in the next section.

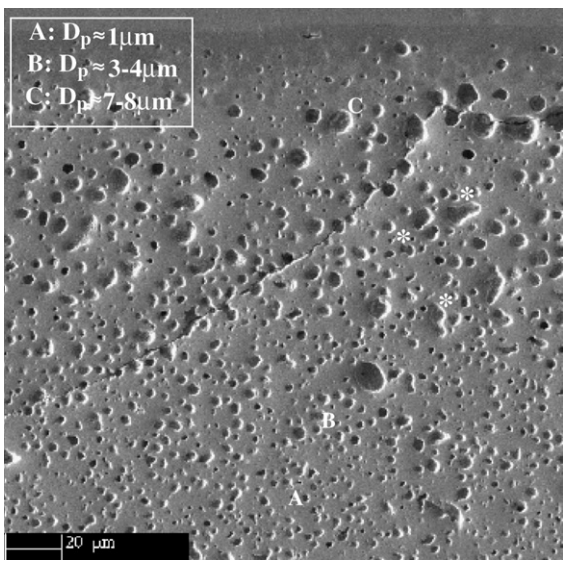

Fig. 2. Pore distribution in the high-burnup structure: SEM picture showing formation of three classes (A, B and C) of pore sizes ranging from ≈1 μm to ≈15 μm.

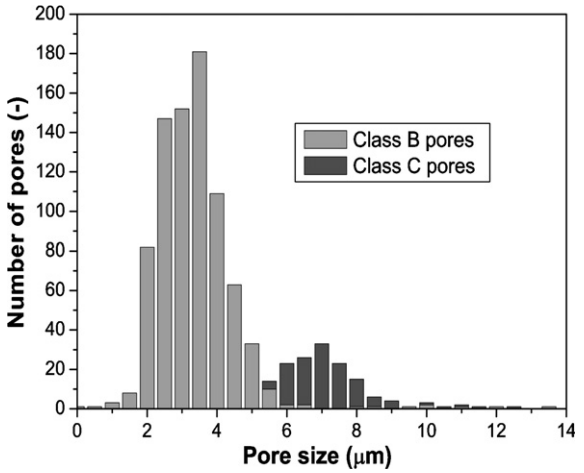

Fig. 3. Histograms of the class B and C pore size distributions taken from several high-burnup fuel regions.

4. Interpretation of the measurements

A simple analytical model is developed to interpret the observations. First, we summarize the major results from the EPMA and SEM measurements:

(1) The HBS is characterized by populations of standard 1 μm pores and by families of less numerous pores with sizes distributed around ≈3–4 μm and ≈7–8 μm (class B and C pores).
(2) The spreading of the large and extra-large pore distributions is wider than that of the standard HBS pores (class A pores).
(3) The extra large pores are located in the very fuel rim, while the intermediate size pores are concentrated in more internal parts of the HBS.
(4) The porosities of the HBS and of the UHBS are comparable.

4.1. Formation of the intermediate size pores

The formation of the intermediate pores (class B) can be modeled as resulting from relaxation of class A pores, which have an initial overpressurization Δp_i. Therefore, a growth mechanism driven by vacancy diffusion is considered to be sufficient to relax the excess gas free energy accumulated in such

overpressurized pores. Thus, the following pore growth kinetics equations can be written as

$$\frac{\partial R}{\partial t} = \left(\frac{\Omega}{R}\right)(D_v C_v - D_i C_i)\left[1 - \exp\left(-\frac{\Omega \Delta p}{k_B T}\right)\right], \quad (1)$$

$$\Delta p = p - \frac{2\gamma}{R}, \quad (2)$$

$$p = \frac{n k_B T}{V - n\Omega}. \quad (3)$$

Eq. (1) describes growth as driven by vacancy and interstitial diffusion, for a pore with an excess pressure Δp. Values for the vacancy and interstitial concentrations, C_v and C_i, and for the diffusion coefficients, D_v and D_i, are taken from Ref. [4], as well as the vacancy volume, Ω, which is 8.5E6 pm^3/atom. The value of the surface tension γ is taken as 1 J/m^2. Moreover, we use the Van-der-Waals model for the pore gas equation of state (Eq. (3)): in this equation, the temperature T is set to 750 K. Furthermore, once the pore pressure is assigned, the number of gas atoms per pore, n, can be directly inferred.

We consider a HBS pore of 1 μm size with overpressurizations ranging from 30 MPa to 200 MPa. Eqs. (1)–(3) are then applied to determine the new dimensions of the pore as a result of the equilibration process. Fig. 4 shows the evolution of the pore overpressurization as a function of pore size during the relaxation process. When the initial excess pressure is set around 50–70 MPa, growth of the original 1 μm pore is activated producing pores at equilibrium with sizes of 3–4 μm, such as those observed in the EPMA and SEM snapshots. We stress here, that values from 50 MPa to 70 MPa are reasonable estimations for the pressure of pores in the high-burnup fuel [10,11]. In fact, the gas concentration in the matrix is ≈0.2 wt%, while the gas produced in the HBS can be estimated as 1.5 wt%. Therefore, assuming that ≈1.3 wt% gas is in the 1 μm pores and using the Van-der-Waals equation of state for $T = 750$ K and a porosity of ≈10%, one obtains a pore pressure of ≈60 MPa, in good agreement with our assumption. Moreover, Fig. 4 shows that in order to produce extra large pores with diameters of 7–8 μm exclusively by vacancy-assisted growth of the original HBS pores, a very high initial overpressurization (>200 MPa) would be needed. However, the direct growth would not explain the observed reduction of the number of pores in the UHBS. Therefore, direct creation of the class C pores by growth is considered improbable without the assist of pore coalescence processes.

Fig. 5 shows the distribution of pores obtained after applying the growth model to an initial population whose size is normally distributed around 1 μm. Two initial overpressures are considered: $\Delta p = 60$ MPa and $\Delta p = 200$ MPa. The pore growth equations yield final distributions with larger variances than the original one. The variances of the distributions increase with the initial pore pressure. Note that the full width at half maximum of the distribution centered around $D_p \approx 3.5$ μm is calculated to be about 2 μm in fair agreement with the value inferred from Fig. 3.

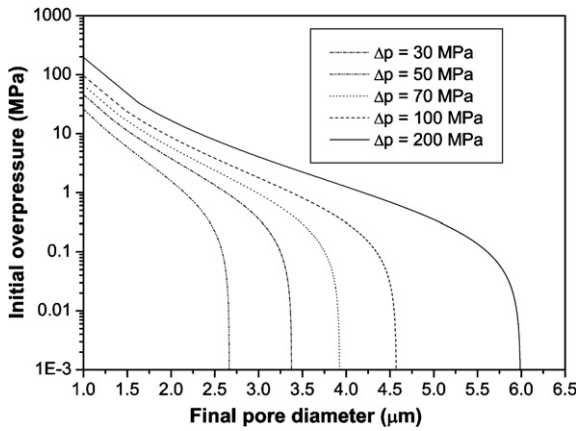

Fig. 4. Pore overpressurization as a function of the diameter for 1 μm pores undergoing growth and characterized by different values of the initial pressure.

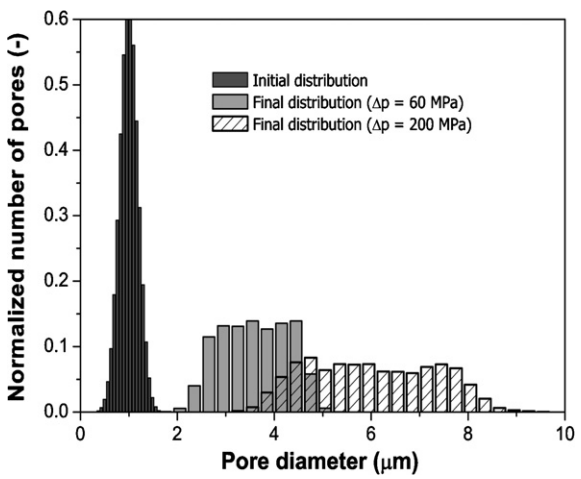

Fig. 5. Final pore size distributions obtained after growth of a Gaussian pore population of ≈1 μm size for two initial overpressurizations: $\Delta p = 60$ MPa and $\Delta p = 200$ MPa.

4.2. Formation of the extra large pores

The EPMA and SEM observations indicate that the porosity of the UHBS region is comparable to that of the more internal HBS, which is characterized by both the intermediate size and the original pores. Such result can be used to formulate a porosity conservation condition giving the time evolution of the number of interacting pores. Thus, the following equations can be written:

$$\frac{\partial(N_p V_p)}{\partial t} = 0, \tag{4}$$

$$\frac{\partial N_p}{\partial t} = -\left(\frac{A_p}{V_p}\right)\left(\frac{\partial R}{\partial t}\right), \tag{5}$$

where N_p is the number of neighbor pores, i.e. pores, which are able to interact by, for example, coalescence, and A_p and V_p are, respectively, the surface and volume of the pores (note that Eq. (5) assumes spherical pores). The time derivative of the pore radius in Eq. (5) is given by Eq. (1). Therefore, the pore evolution is considered to be driven by both vacancy induced growth and pore coalescence.

We assume that after an initial stage of growth leading to an increase of porosity, pore coalescence processes take place, which reduce the total population of pores, while increasing the pore size due to the assisting effect of pore growth driven by vacancy diffusion. Therefore, we consider slightly overpressurized class B pores undergoing coalescence via Eqs. (1)–(5). We assume that such pores are characterized by initial pressures ranging between 2 MPa and 6 MPa. Such initial overpressurization can be due to the continuous flow of gas atoms into the pores by fission, which is partly counterbalanced by the vacancy flux. Alternatively, one could imagine that during the growth stage, interacting intermediate size pores, which have not yet exhausted their original excess pressure, start to coalesce due to their proximity [12]. Examples of pores undergoing coalescence can be seen in the SEM snapshot reported in Fig. 2 (specifically, the pores marked with an asterisk).

Fig. 6 shows locus plots of the number of pores, normalized to the initial value, as a function of the evolving pore diameter D_p, which is expressed in a dimensionless form using the initial pore overpressure, Δp and the surface tension, γ. A parameterization with respect to the initial excess pore pressure is also displayed. As expected, the final pore diameters, D_p^f, reached after application of Eqs. (4) and (5) and the vacancy diffusion model for bubble growth are larger the higher the initial pore pressure. For $\Delta p \approx 5$–6 MPa the final pore diameter is of the order of 6–8 μm, a size typical of the extra large pores of the UHBS. Moreover, for this case, the ratio N_p/N_p^0 ranges between 0.05 and 0.15. Such result compares reasonably well with the values derived from Fig. 3 for the ratio of the class C and class B pores (this is about 15%). Moreover, if the simple porosity conservation model is applied to a distribution of pore sizes centered around an initial diameter of 3.5 μm, a distribution of pores ranging from ≈4 μm to ≈16 μm is obtained.

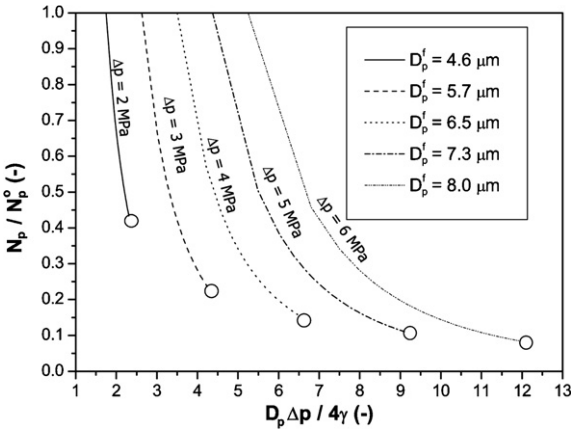

Fig. 6. Locus plots of the fractional number of pores as a function of the pore diameter (expressed in dimensionless units as $D_p \Delta p/4\gamma$) for different initial overpressurizations.

In summary, our simple model interprets the evolution of the porosity in the high-burnup structure sample analyzed at PSI as the result of (1) a growth process, responsible for the formation of 3–4 μm pores, followed by (2) a phase where coalescence of pores can lead to the formation of the extra large pores. In this process vacancy diffusion plays a fundamental role and the pore overpressurization is the main driving force for their evolution. It must be remarked that because the diffusion of vacancies is strongly dependent on temperature and stoichiometry, we expect that such parameters would influence the kinetics of formation of the HBS pores. Specifically, fuel stoichiometry increases towards the fuel rim, due to the larger values of the burnup, may accelerate the pore growth by enhancing the vacancy diffusion rate. Furthermore, the flux of vacancies into the pores depends on their local concentration C_v. We acknowledge that, for simplicity, all these parameters have been taken as constant in

our simple approach since this study focused primarily on capturing the qualitative features of the pore population observed experimentally. However, future work should be devoted to better understand the role of temperature, stoichiometry and vacancy population in driving the evolution of the fuel porosity in the high-burnup structure.

5. Conclusions

In this study the HBS porosity is investigated using both experimental and analytical approaches. Measurements of very high-burnup fuel (≈105 GWd/tHM) samples have been conducted, using EPMA and SEM techniques. Moreover, quantitative methods have been applied to determine the radial distribution of sensitive isotopes in the high-burnup structure. These observations indicate formation of extra-large gas pores of diameters up to 15 μm in the very rim region yielding local porosities of about 22%. Intermediate pores of 3–5 μm size are also obtained, which extend towards more internal regions of the HBS. Furthermore, the traditional HBS and a transition region develop up to 2 mm inside the fuel. A quantitative elemental concentration analysis indicates that the local burnup can reach values up to 300 GWd/tHM in correspondence to the ultra-high burnup region, which features extra large pores. Finally, the pore size distribution for intermediate and large pores is derived: pores of diameters ≈3.5 μm and 7.5 μm occur with higher frequencies than others.

A simple model of porosity evolution has been introduced to interpret the observations. Such model includes equations for vacancy assisted growth and pore coalescence processes, which conserve the porosity. The intermediate size pores are obtained by pure growth of overpressurized pores driven by vacancy flow. In this growth stage the number of pores does not change but the porosity increases until a new population of pores with a larger diameter is generated. The qualitative results of the measurements are reproduced by the model if the initial pore pressure is set to be in the range 50–70 MPa. A second stage is then considered, which prescribes coalescence of the pores under the condition that the total porosity be preserved. In this stage, the model yields formation of a less numerous population of extra large pores. The size of the final pores depends on the pore overpressurization at which the coalescence process starts. The model yields that pore pressures of only 5–6 MPa are sufficient to yield the 7.5 μm pores observed the UHBS.

Acknowledgements

The authors are thankful to Grigori Khvostov, Christian Hellwig and Martin Zimmermann for fruitful discussions. M. Horvath and R. Restani acknowledge the sample preparation work of A. Wälchli and H. Schweikert.

References

[1] J. Spino, K. Vennix, M. Coquerelle, J. Nucl. Mater. 231 (1996) 179.
[2] J. Spino, J. Rest, W. Goll, C.T. Walker, J. Nucl. Mater. 346 (2005) 179.
[3] P. Blair, A. Romano, Ch. Hellwig, R. Chawla, J. Nucl. Mater. 350 (2006) 232.
[4] M. Kinoshita, J. Nucl. Mater. 248 (1997) 185.
[5] Hj. Matzke, J. Spino, J. Nucl. Mater. 248 (1997) 170.
[6] J. Spino, A.D. Stalios, H. Santa Cruz, D. Baron, J. Nucl. Mater. 354 (2006) 66.
[7] C. Ronchi, N. Sheindlin, D. Staicu, M. Kinoshita, J. Nucl. Mater. 327 (2004) 58.
[8] J. Spino, J. Cobos-Sabate, F. Rosseau, J. Nucl. Mater. 322 (2003) 204.
[9] Microanalysis application software. <www.samx.com>.
[10] Yang-Hyun Koo, Byung-Ho Lee, Jin-Sok Cheon, Dong-Seong Sohn, J. Nucl. Mater. 295 (2001) 213.
[11] W. Goll, Ch. Hellwig, P.B. Hoffmann, W. Sauser, J. Spino, C.T. Walker, Int. J. Nucl. Power, 7, in press.
[12] J.R. Willis, R. Bullough, J. Nucl. Mater. 32 (1969) 76.